Frank J. Centinello III

# ANALYSIS OF THE NED AND ECEF COVARIANCE PROPAGATION FOR THE NAVIGATIONAL EXTENDED KALMAN FILTER

University at Buffalo, The State University of New York
Buffalo, New York, United States of America
fjc3@eng.buffalo.edu

**Abstract**

The Extended Kalman Filter (EKF) is the most widely used algorithm for estimation in GPS/INS navigation. The EKF is a sequential state estimator for use with nonlinear systems. The navigational EKF can be programmed in geocentric (ECEF) and navigational (latitude, longitude, and altitude) coordinates. This is a presentation of the affect the choice of coordinate frame has on the covariance-propagation of the EKF. For the EKF, a model's error dynamics are approximated using a first-order Taylor series representation of the equations of motion. For this study, the choice of reference frame greatly affects the complexity of this approximation. Key filter differences are presented, and the results of filter performance tests are shown.

## 1 Introduction

Estimation of inertial measurement unit (IMU) errors is one of the primary goals of navigational filtering. Upon loss of GPS signals, an inertial navigation system (INS) with well-estimated measurement parameters can sometimes provide accurate position information until GPS updates are possible again. The choice of reference frame in navigation is arbitrary, but may be swayed by prior knowledge of navigational accuracy and computational performance. The two frames considered in this work are the ECEF and North-East-Down (NED) coordinate systems. The ECEF frame represents a cartesian position with respect to the center of Earth, and the NED frame is composed of the geographic latitude, longitude, and height. Reasons for choosing either span computational efficiency to ease of interpretation.

In the case of navigational estimation, GPS signals are used to determine the errors associated with inertial measurement units (IMUs). IMU measurements are subject to bias, scaling and misalignment error [1]. These errors cause inaccuracy in velocity and position calculations due to the fact that IMU data are integrated over time. Even with a good initial condition, integrated sensor errors can result in large position and velocity errors over a short amount of time. As an INS provides velocity and position data through the integration of IMU measurements, GPS position measurements can be used to estimate IMU errors [2],[3],[4].

The scope of this work is a test of the extended Kalman filter (EKF) for navigation programmed in different reference frames. The EKF is a version of the Kalman filter used estimate the dynamics of nonlinear systems [2]. The EKF attempts to approximate the dynamics of a nonlinear system using the first order term of a Taylor-series expansion of the equations of motion. Another principal assumption of the EKF derivation is that the Gaussian nature of input noise can be preserved through a linearization of the system dynamics. For these reasons, the EKF is inherently suboptimal, and its degree of estimation accuracy can be difficult to quantify [5], [6]. The choice of reference frame affects the filter observability by changing the kinematic equations of motion and directly influencing the covariance (estimation error) propagation segment of the algorithm.

The EKF versions will be compared in terms of navigation accuracy through observation of the estimate errors and covariance. Also, the results of a study of a nonlinearity test performed on the navigational EKFs are presented. A similar study has been performed with actual navigational hardware by Wei [7]. Wei's analysis covers computational

performance and estimation accuracy, and is limited to the performance characteristics of hardware. These characteristics most likely include sampling intervals and the use of a different programming language.

A brief overview of reference frames and filtering is provided in the next section. The extended filter equations for navigation in the NED and ECEF frames are then provided and followed by simulation results and conclusions.

## 2    Reference Frames

Navigational estimation requires the use of several frames. They are illustrated in Figure 1. First, the Earth-Centered-Inertial (ECI) frame is concentric with Earth, and is fixed in space, meaning its orientation is constant with respect to the celestial sphere [3]. Representations in ECI coordinates will have the superscript $I$ (e.g., $\mathbf{r}^I$). The next reference frame is the Earth-Centered-Earth-Fixed (ECEF) frame, denoted with the vectors $\{\hat{\mathbf{e}}_1, \hat{\mathbf{e}}_2, \hat{\mathbf{e}}_3\}$ in Figure 1. This frame is an Earth-centered frame which rotates with the Earth. Vectors represented in the ECEF frame will take the superscript $E$, (e.g., $\mathbf{r}^E$).

The North-East-Down (NED) frame is denoted by $\{\hat{\mathbf{n}}, \hat{\mathbf{e}}, \hat{\mathbf{d}}\}$. Its unit vectors represent their descriptive directions for a point on the surface of the Earth model. The $\hat{\mathbf{n}}$ axis points to true North, $\hat{\mathbf{e}}$ points East, and $\hat{\mathbf{d}}$ completes the coordinate system, in Figure 1. The reason $\hat{\mathbf{d}}$ is described in this way rather than said to point downward is because of the elliptical Earth model chosen. In this work, a local NED frame is defined about which an arbitrary vehicle navigates. NED frame representations will be denoted with the superscript $N$, (e.g., $\mathbf{r}^N$). The reference frames detailed above are illustrated in Figure 1.

Finally, the body frame will be denoted by $\{\hat{\mathbf{b}}_1, \hat{\mathbf{b}}_2, \hat{\mathbf{b}}_3\}$. This frame's origin and directions are fixed to the navigating vehicle. Unit vector directions are arbitrary. Body frame representations will be denoted with the superscript $B$, (e.g., $\mathbf{r}^B$).

Details of transformation between these coordinate bases are omitted from this paper for brevity. A full derivation is presented in [3].
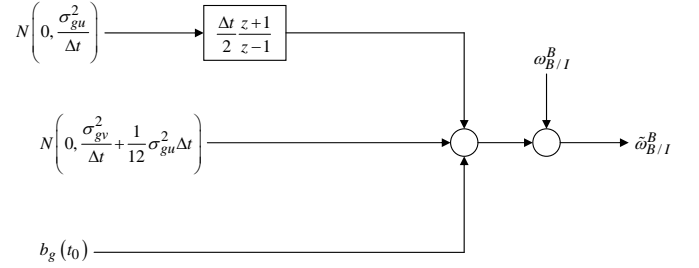


Figure 2: Schematic of IMU Measurement Model

## 3    Measurement Models

In this section, the measurement models used in this work will be presented. First, the GPS pseudorange is defined as the norm of the radius vector between the user and the satellite [1], [3]. The measurement is the the sum of the pseudorange, clock bias, $b_c$, and $v$, a zero-mean Gaussian white noise process which represents the measurement noise:

$$\tilde{\rho}_i = \|\mathbf{R}_i^E - \mathbf{r}^E\| + b_c + v, i = 1, 2, \ldots, n \qquad (1)$$

Here, $\mathbf{r}^E$ is the position of the receiver in ECEF coordinates, and $\mathbf{R}^E$ is the position of the GPS satellite in ECEF coordinates. This is illustrated in Figure 1. The GPS clock bias is denoted with $b_c$, and is representative of nearly constant errors in the satellite's atomic clock [2].

Derivations of models for the gyros and accelerometers are available in [3] and [8]. The gyro measurement model is the sum of the true rate, $\boldsymbol{\omega}_{B/I}^B$ and bias, $\mathbf{b}_g$.

$$\tilde{\boldsymbol{\omega}}_{B/I}^B = \boldsymbol{\omega}_{B/I}^B + \mathbf{b}_g + \boldsymbol{\eta}_{gv} \qquad (2a)$$

$$\dot{\mathbf{b}}_g = \boldsymbol{\eta}_{gu} \qquad (2b)$$

The final terms $\boldsymbol{\eta}_{gv}$, and $\boldsymbol{\eta}_{gu}$ are zero-mean Gaussian processes which simulate measurement noise and gyro bias drift, respectively. Their spectral densities are given by $\sigma_{gv}^2 I_{3\times3}$ and $\sigma_{gu}^2 I_{3\times3}$, respectively. The gyro model is illustrated in Fig. 2. Similarly, the accelerometer measurement model is given by:

$$\tilde{\mathbf{a}}^B = \mathbf{a}^B + \mathbf{b}_a + \boldsymbol{\eta}_{av} \qquad (3a)$$

$$\dot{\mathbf{b}}_a = \boldsymbol{\eta}_{au} \qquad (3b)$$

Again, $\boldsymbol{\eta}_{av}$, and $\boldsymbol{\eta}_{au}$ are zero-mean Gaussian processes to simulate measurement noise and accelerometer bias drift, respectively. Their spectral
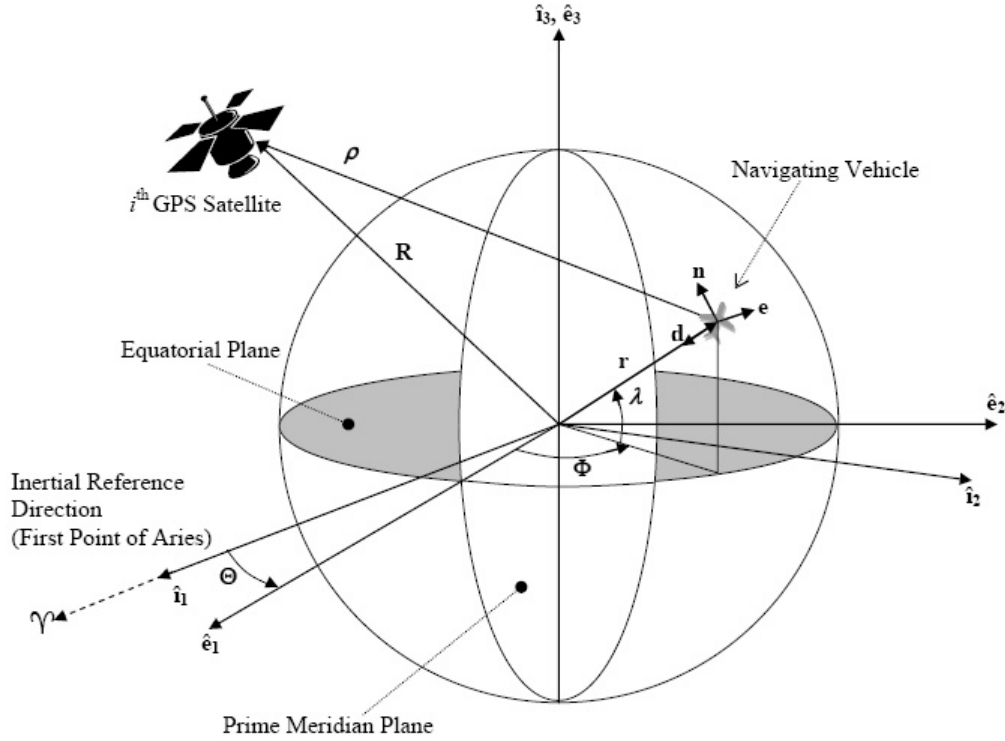
Figure 1: Definitions of Various Reference Frames

densities are given by $\sigma_{av}^2 I_{3\times3}$ and $\sigma_{au}^2 I_{3\times3}$, respectively.

Modeling of measurement signals is difficult. This is because manufacturers give information about the measurement noise values, but not the drift rates. Furthermore, measurement signals are continuous, which are impossible to simulate with computers. A discrete-time approximation of the signals is possible with the use of the spectral densities. This is shown in Figure 2, where $N\left(0, \sigma^2\right)$ are zero-mean normal distributions with variance $\sigma^2$ [9]. This measurement model is used for both gyro and accelerometer measurements.

# 4  Navigational Filtering

The extended Kalman filter for navigation in the ECEF and NED frames will now be presented. A derivation of the EKF is available in [2]. The EKF intialization, update, and propagation are shown briefly in Table 1. The initialization, gain computation, and update are the same for both versions. The equations for the measurement and kinematics are used for the measurement model and propaga-

tion of the state estimate. These will be shown in detail. Next, the linearization of these will be presented. These are the differences between the parameterization of the filter in the ECEF and NED frames.

## 4.1  The ECEF Filter

First, the kinematic equations in the ECEF frame are given by:

$$\dot{\mathbf{q}} = \frac{1}{2}\Xi(\mathbf{q})\boldsymbol{\omega}_{B/E}^B \tag{4a}$$

$$\boldsymbol{\omega}_{B/E}^B = (\tilde{\boldsymbol{\omega}}_{B/I}^B - \mathbf{b}_g - \boldsymbol{\eta}_v) - A_E^B(\mathbf{q})\boldsymbol{\omega}_{E/I}^E \tag{4b}$$

$$\ddot{\mathbf{r}}^E = -[\boldsymbol{\omega}_{E/I}^E\times][\boldsymbol{\omega}_{E/I}^E\times]\mathbf{r}^E - 2[\boldsymbol{\omega}_{E/I}^E\times]\dot{\mathbf{r}}^E \\ +A_B^E(\mathbf{q})\mathbf{a}^B + \mathbf{g}^E \tag{4c}$$

$$\mathbf{a}^B = (\tilde{\mathbf{a}}^B - \mathbf{b}_a - \boldsymbol{\eta}_{av}) \tag{4d}$$

$$\mathbf{g}^E = \frac{-\mu}{\|\mathbf{r}^E\|^3}\mathbf{r}^E + \mathbf{a}_{J_2}^E(\mathbf{r}^E) \tag{4e}$$

$$\dot{\mathbf{b}}_g = \boldsymbol{\eta}_{gu} \tag{4f}$$

3

Table 1: Continuous-Discrete Extended Kalman Filter

| Model | $\dot{\mathbf{x}}_{k+1} = \mathbf{f}(\mathbf{x}(t), \mathbf{u}, (t), t) + G(t)\mathbf{w}(t), \mathbf{w}(t) \sim N(\mathbf{0}, Q(t))$ |
|---|---|
| | $\tilde{\mathbf{y}}_k = \mathbf{h}(\mathbf{x})_k + \mathbf{v}_k, \mathbf{v}_k \sim N(\mathbf{0}, R_k)$ |
| Initialize | $\hat{\mathbf{x}}(t_0) = \hat{\mathbf{x}}_0$ |
| | $P_0 = E\{\tilde{\mathbf{x}}_0 \tilde{\mathbf{x}}_0^T\}$ |
| Gain | $K_k = P_k^- H_k^T(\hat{\mathbf{x}}_k^-)[H_k(\hat{\mathbf{x}}_k^-)P_k^- H_k(\hat{\mathbf{x}}_k^-)^T + R_k]^{-1}$ |
| | $H_k(\hat{\mathbf{x}}_k^-) \equiv \frac{\partial \mathbf{h}}{\partial \mathbf{x}}\Big|_{\hat{\mathbf{x}}_k^-}$ |
| Update | $\hat{\mathbf{x}}_k^+ = \hat{\mathbf{x}}_k^- + K_k[\tilde{\mathbf{y}}_k - \mathbf{h}(\hat{\mathbf{x}}_k^-)]$ |
| | $P_k^+ = [I - K_k H_k(\hat{\mathbf{x}}_k^-)]P_k^-$ |
| Propagation | $\dot{\hat{\mathbf{x}}}(\mathbf{t}) = \mathbf{f}(\hat{\mathbf{x}}(\mathbf{t}), \mathbf{u}(\mathbf{t}), \mathbf{t})$ |
| | $\dot{P} = F(\hat{\mathbf{x}}(t), t)P(t) + P(t)F^T(\hat{\mathbf{x}}(t), t) + G(t)Q(t)G^T(t)$ |
| | $F(\hat{\mathbf{x}}(t), t) \equiv \frac{\partial \mathbf{f}}{\partial \mathbf{x}}\Big|_{\hat{\mathbf{x}}(t)}$ |

$$\dot{\mathbf{b}}_a = \boldsymbol{\eta}_{au} \qquad (4g)$$

$$\dot{b}_c = 0 \qquad (4h)$$

The first vector state $\mathbf{q}$ is an an attitude quaternion which represents the body's orientation with respect to the ECEF frame. This is a four-dimensional representation with nonsingular kinematics [2]. Next, the angular velocity between the two frames is represented by $\boldsymbol{\omega}_{B/E}^B$. Acceleration is described by $\ddot{\mathbf{r}}^E$. The ECEF gravity model is provided in $\mathbf{g}^E$, where $\mathbf{a}_{J_2}^E$ is the contribution from the Earth ellipsoidal nature, and is described in [10].

Here $\mathbf{b}_g$ and $\mathbf{b}_a$ are the gyro and accelerometer biases described in Eqns. (2) and (3). The GPS clock bias is represented as $b_c$. Next, the state estimate is given by:

$$\dot{\hat{\mathbf{q}}} = \frac{1}{2}\Xi(\hat{\mathbf{q}})\hat{\boldsymbol{\omega}}_{B/E}^B \qquad (5a)$$

$$\hat{\boldsymbol{\omega}}_{B/E}^B = (\tilde{\boldsymbol{\omega}}_{B/I}^B - \hat{\mathbf{b}}_g) - A_E^B(\hat{\mathbf{q}})\boldsymbol{\omega}_{E/I}^E \qquad (5b)$$

$$\ddot{\hat{\mathbf{r}}}^E = -[\boldsymbol{\omega}_{E/I}^E \times][\boldsymbol{\omega}_{E/I}^E \times]\hat{\mathbf{r}}^E - 2[\boldsymbol{\omega}_{E/I}^E \times]\dot{\hat{\mathbf{r}}}^E$$
$$+ A_B^E(\hat{\mathbf{q}})\hat{\mathbf{a}}^B + \hat{\mathbf{g}}^E$$
$$(5c)$$

$$\hat{\mathbf{a}}^B = (\tilde{\mathbf{a}}^B - \hat{\mathbf{b}}_a) \qquad (5d)$$

$$\hat{\mathbf{g}}^E = \frac{-\mu}{\|\hat{\mathbf{r}}^E\|^3}\hat{\mathbf{r}}^E + \mathbf{a}_{J_2}^E(\hat{\mathbf{r}}^E) \qquad (5e)$$

$$\dot{\hat{\mathbf{b}}}_g = \mathbf{0} \qquad (5f)$$

$$\dot{\hat{\mathbf{b}}}_a = \mathbf{0} \qquad (5g)$$

$$\dot{b}_c = 0 \qquad (5h)$$

Here, it is most important to note that the attitude matrix is present in the position equations, which allows the estimation of attitude with position measurements. The GPS measurement model is provided by Eqn. (1). That is, $\mathbf{h}(\mathbf{x}) = \tilde{\rho}$. For the measurement, the following linearization about the state is obtained:

$$H_k = \begin{bmatrix} 0_{1\times 3} & -\frac{\mathbf{R}_i^E - \hat{\mathbf{r}}_k^E}{\|\mathbf{R}_i^E - \hat{\mathbf{r}}_k^E\|} & 0_{1\times 9} & 1 \end{bmatrix} \qquad (6)$$

The state vector, state-error vector, process noise vector and process noise spectral density matrix are

4

given by:

$$\mathbf{x} \equiv \begin{bmatrix} \mathbf{q} \\ \mathbf{r}^E \\ \dot{\mathbf{r}}^E \\ \mathbf{b}_g \\ \mathbf{b}_a \\ b_c \end{bmatrix}, \Delta\mathbf{x} \equiv \begin{bmatrix} \boldsymbol{\delta\alpha} \\ \Delta\mathbf{r}^E \\ \Delta\dot{\mathbf{r}}^E \\ \Delta\mathbf{b}_g \\ \Delta\mathbf{b}_a \\ \Delta b_c \end{bmatrix}, \mathbf{w} = \begin{bmatrix} \boldsymbol{\eta}_{gv} \\ \boldsymbol{\eta}_{gu} \\ \boldsymbol{\eta}_{av} \\ \boldsymbol{\eta}_{au} \end{bmatrix}$$

(7a)

$$Q = \begin{bmatrix} \sigma_{gv}^2 I_{3\times3} & 0_{3\times3} & 0_{3\times3} & 0_{3\times3} & 0_{3\times1} \\ 0_{3\times3} & \sigma_{gu}^2 I_{3\times3} & 0_{3\times3} & 0_{3\times3} & 0_{3\times1} \\ 0_{3\times3} & 0_{3\times3} & \sigma_{av}^2 I_{3\times3} & 0_{3\times3} & 0_{3\times1} \\ 0_{3\times3} & 0_{3\times3} & 0_{3\times3} & \sigma_{au}^2 I_{3\times3} & 0_{3\times1} \\ 0_{1\times3} & 0_{1\times3} & 0_{1\times3} & 0_{1\times3} & 0 \end{bmatrix}$$

(7b)

The approximations expressed in the linearized kinematics from [3] with the gyro and accelerometer bias equations from Eqns. (2) and (3) are used in the linear propagation of the errors represented as:

$$\Delta\dot{\mathbf{x}} = F\Delta\mathbf{x} + G\mathbf{w} \tag{8}$$

where $F$ and $G$ are given by:

$$F \equiv \begin{bmatrix} F_{11} & 0_{3\times3} & 0_{3\times3} & F_{14} & 0_{3\times3} & 0_{3\times1} \\ 0_{3\times3} & 0_{3\times3} & I_{3\times3} & 0_{3\times3} & 0_{3\times3} & 0_{3\times1} \\ F_{31} & F_{32} & F_{33} & 0_{3\times3} & F_{35} & 0_{3\times1} \\ 0_{3\times3} & 0_{3\times3} & 0_{3\times3} & 0_{3\times3} & 0_{3\times3} & 0_{3\times1} \\ 0_{3\times3} & 0_{3\times3} & 0_{3\times3} & 0_{3\times3} & 0_{3\times3} & 0_{3\times1} \\ 0_{1\times3} & 0_{1\times3} & 0_{1\times3} & 0_{1\times3} & 0_{1\times3} & 0 \end{bmatrix}$$

(9a)

$$G \equiv \begin{bmatrix} -I_{3\times3} & 0_{3\times3} & 0_{3\times3} & 0_{3\times3} & 0_{3\times1} \\ 0_{3\times3} & 0_{3\times3} & 0_{3\times3} & 0_{3\times3} & 0_{3\times1} \\ 0_{3\times3} & 0_{3\times3} & -A_B^E(\hat{\mathbf{q}}) & 0_{3\times3} & 0_{3\times1} \\ 0_{3\times3} & I_{3\times3} & 0_{3\times3} & 0_{3\times3} & 0_{3\times1} \\ 0_{3\times3} & 0_{3\times3} & 0_{3\times3} & I_{3\times3} & 0_{3\times1} \\ 0_{1\times3} & 0_{1\times3} & 0_{1\times3} & 0_{1\times3} & 1 \end{bmatrix}$$

(9b)

where $F$ is populated with:

$$F_{11} = -[(\hat{\boldsymbol{\omega}}_{B/E}^B + A_E^B(\hat{\mathbf{q}})\boldsymbol{\omega}_{E/I}^E)\times] \tag{10a}$$

$$F_{14} = -I_{3\times3} \tag{10b}$$

$$F_{31} = -A_B^E(\hat{\mathbf{q}})[\hat{\mathbf{a}}^B\times] \tag{10c}$$

$$F_{32} = U(\hat{\mathbf{r}}^E) - [\boldsymbol{\omega}_{E/I}^E\times][\boldsymbol{\omega}_{E/I}^E\times] \tag{10d}$$

$$F_{33} = -2[\boldsymbol{\omega}_{E/I}^E\times] \tag{10e}$$

$$F_{35} = -A_B^E(\hat{\mathbf{q}}) \tag{10f}$$

## 4.2 The NED Filter

To parameterize the EKF for navigational estimation in the NED frame, we will begin with the truth equations:

$$\dot{\mathbf{q}} = \frac{1}{2}\Xi(\mathbf{q})\boldsymbol{\omega}_{B/N}^B \tag{11a}$$

$$\dot{\lambda} = \frac{v_N}{R_\lambda + h} \tag{11b}$$

$$\dot{\Phi} = \frac{v_E}{(R_\Phi + h)\cos\lambda} \tag{11c}$$

$$\dot{h} = -v_D \tag{11d}$$

$$\dot{v}_N = -\left[\frac{v_E}{(R_\Phi + h)\cos\lambda} + 2\boldsymbol{\omega}_e\right]v_E\sin\lambda \\ + \frac{v_N v_D}{(R_\lambda + h)} + a_N$$

(11e)

$$\dot{v}_E = \left[\frac{v_E}{(R_\Phi + h)\cos\lambda} + 2\omega_e\right]v_N\sin\lambda \\ + \frac{v_E v_D}{R_\Phi + h} + 2\omega_e v_D\cos\lambda + a_E$$

(11f)

$$\dot{v}_D = -\frac{v_E^2}{R_\Phi + h} - \frac{v_N^2}{R_\lambda + h} - 2\omega_e v_E\cos\lambda \\ + g + a_D$$

(11g)

with the following inputs:

$$\boldsymbol{\omega}_{B/N}^B = (\tilde{\boldsymbol{\omega}}_{B/I}^B - \mathbf{b}_g - \boldsymbol{\eta}_{gv}) - A_N^B(\mathbf{q})\boldsymbol{\omega}_{N/I}^N \tag{12a}$$

$$\mathbf{a}^B = \tilde{\mathbf{a}}^B - \mathbf{b}_a - \boldsymbol{\eta}_{gv} \tag{12b}$$

Here, the $x$- and $z$- coordinates for a point $on$ the Earth ellipsoid are given by [11]:

$$R_\lambda = \frac{a(1 - e^2)}{(1 - e^2\sin^2\lambda)^{3/2}} \tag{13a}$$

$$R_\Phi = \frac{a}{(1 - e^2\sin^2\lambda)^{1/2}} \tag{13b}$$

The first state derivative is the kinematics of the quaternion representing the attitude between the

**NED and body frames.** The angular rate given here is $\omega_{B/N}^B$, which describes rotation between the NED and body frames in body coordinates. Next come the position in the form of geographic latitude, longitude, and height: $\mathbf{p} = \begin{bmatrix} \lambda & \Phi & h \end{bmatrix}^T$. The accelerations are those along the axes of the NED frame.

In the NED frame, the gravity model is given by:

$$g = A\left(1 + B\sin^2\lambda - C\sin^2 2\lambda\right) - \left(D - E\sin^2\lambda\right)h + Fh^2 \tag{14}$$

where the coefficients are given in Table 2.

The estimated states are given by:

$$\dot{\hat{\mathbf{q}}} = \frac{1}{2}\Xi\left(\hat{\mathbf{q}}\right)\hat{\omega}_{B/N}^B \tag{15a}$$

$$\dot{\hat{\lambda}} = \frac{\hat{v}_N}{R_\lambda + \hat{h}} \tag{15b}$$

$$\dot{\hat{\Phi}} = \frac{\hat{v}_E}{\left(R_\Phi + \hat{h}\right)\cos\hat{\lambda}} \tag{15c}$$

$$\dot{\hat{h}} = -\hat{v}_D \tag{15d}$$

$$\dot{\hat{v}}_N = -\left[\frac{\hat{v}_E}{\left(R_\Phi + \hat{h}\right)\cos\hat{\lambda}} + 2\omega_e\right]\hat{v}_E\sin\hat{\lambda} + \frac{\hat{v}_N\hat{v}_D}{\left(R_\lambda + \hat{h}\right)} + \hat{a}_N \tag{15e}$$

$$\dot{\hat{v}}_E = \left[\frac{\hat{v}_E}{\left(R_\Phi + \hat{h}\right)\cos\hat{\lambda}} + 2\omega_e\right]\hat{v}_N\sin\hat{\lambda} + \frac{\hat{v}_E\hat{v}_D}{R_\Phi + \hat{h}} + 2\omega_e\hat{v}_D\cos\hat{\lambda} + \hat{a}_E \tag{15f}$$

$$\dot{\hat{v}}_D = -\frac{\hat{v}_E^2}{R_\Phi + \hat{h}} - \frac{\hat{v}_N^2}{R_\lambda + \hat{h}} - 2\omega_e\hat{v}_E\cos\hat{\lambda} + \hat{g} + \hat{a}_D \tag{15g}$$

$$\hat{\mathbf{a}}^N = \begin{bmatrix} \hat{a}_N \\ \hat{a}_E \\ \hat{a}_D \end{bmatrix} = A_B^N(\hat{\mathbf{q}})\hat{\mathbf{a}}^B \tag{15h}$$

$$\hat{\mathbf{a}}^B = \tilde{\mathbf{a}}^B - \hat{\mathbf{b}}_a \tag{15i}$$

$$\dot{\hat{\mathbf{b}}}_g = \mathbf{0} \tag{15j}$$

$$\dot{\hat{\mathbf{b}}}_a = \mathbf{0} \tag{15k}$$

$$\dot{\hat{b}}_c = 0 \tag{15l}$$

The measurement update is provided by Eq. (1), making it linearization with respect to the state:

$$H_k = \begin{bmatrix} 0_{1\times 3} & -\frac{\mathbf{R}_i^E - \hat{\mathbf{r}}_k^E}{\|\mathbf{R}_i^E - \hat{\mathbf{r}}_k^E\|}\frac{\partial \boldsymbol{r}^E}{\partial \boldsymbol{p}} & 0_{1\times 9} & 1 \end{bmatrix} \tag{16}$$

Next, the state vector, error vector, process noise vector and process noise spectral density matrix are given by:

$$\mathbf{x} \equiv \begin{bmatrix} \mathbf{q} \\ \mathbf{p} \\ \mathbf{v}^N \\ \mathbf{b}_g \\ \mathbf{b}_a \\ b_c \end{bmatrix}, \Delta\mathbf{x} \equiv \begin{bmatrix} \boldsymbol{\delta\alpha} \\ \Delta\mathbf{p} \\ \Delta\mathbf{v}^N \\ \Delta\mathbf{b}_g \\ \Delta\mathbf{b}_a \\ \Delta b_c \end{bmatrix}, \mathbf{w} = \begin{bmatrix} \eta_{gv} \\ \eta_{gu} \\ \eta_{av} \\ \eta_{au} \end{bmatrix} \tag{17a}$$

and:

$$Q = \begin{bmatrix} \sigma_{gv}^2 I_{3\times 3} & 0_{3\times 3} & 0_{3\times 3} & 0_{3\times 3} & 0_{3\times 1} \\ 0_{3\times 3} & \sigma_{gu}^2 I_{3\times 3} & 0_{3\times 3} & 0_{3\times 3} & 0_{3\times 1} \\ 0_{3\times 3} & 0_{3\times 3} & \sigma_{av}^2 I_{3\times 3} & 0_{3\times 3} & 0_{3\times 1} \\ 0_{3\times 3} & 0_{3\times 3} & 0_{3\times 3} & \sigma_{au}^2 I_{3\times 3} & 0_{3\times 1} \\ 0_{1\times 3} & 0_{1\times 3} & 0_{1\times 3} & 0_{1\times 3} & 0 \end{bmatrix} \tag{17b}$$

For the NED equations $F$ and $G$ are given by:

$$F \equiv \begin{bmatrix} F_{11} & F_{12} & F_{13} & F_{14} & 0_{3\times 3} & 0_{3\times 1} \\ 0_{3\times 3} & F_{22} & F_{23} & 0_{3\times 3} & 0_{3\times 3} & 0_{3\times 1} \\ F_{31} & F_{32} & F_{33} & 0_{3\times 3} & F_{35} & 0_{3\times 1} \\ 0_{3\times 3} & 0_{3\times 3} & 0_{3\times 3} & 0_{3\times 3} & 0_{3\times 3} & 0_{3\times 1} \\ 0_{3\times 3} & 0_{3\times 3} & 0_{3\times 3} & 0_{3\times 3} & 0_{3\times 3} & 0_{3\times 1} \\ 0_{1\times 3} & 0_{1\times 3} & 0_{1\times 3} & 0_{1\times 3} & 0_{1\times 3} & 0 \end{bmatrix} \tag{18a}$$

and

$$G \equiv \begin{bmatrix} -I_{3\times 3} & 0_{3\times 3} & 0_{3\times 3} & 0_{3\times 3} & 0_{3\times 1} \\ 0_{3\times 3} & 0_{3\times 3} & 0_{3\times 3} & 0_{3\times 3} & 0_{3\times 1} \\ 0_{3\times 3} & 0_{3\times 3} & -A_B^N(\hat{\mathbf{q}}) & 0_{3\times 3} & 0_{3\times 1} \\ 0_{3\times 3} & I_{3\times 3} & 0_{3\times 3} & 0_{3\times 3} & 0_{3\times 1} \\ 0_{3\times 3} & 0_{3\times 3} & 0_{3\times 3} & I_{3\times 3} & 0_{3\times 1} \\ 0_{1\times 3} & 0_{1\times 3} & 0_{1\times 3} & 0_{1\times 3} & 1 \end{bmatrix} \tag{18b}$$

6

where $F$ is populated with:

$$F_{11} = -\left[(\tilde{\omega}_{B/I}^B - \hat{\mathbf{b}}_g)\times\right] \tag{19a}$$

$$F_{12} = -A_N^B(\hat{\mathbf{q}})\frac{\partial \omega_{N/I}^N}{\partial \mathbf{p}}\bigg|_{\hat{\mathbf{p}},\hat{\mathbf{v}}^N} \tag{19b}$$

$$F_{13} = -A_N^B(\hat{\mathbf{q}})\frac{\partial \omega_{N/I}^N}{\partial \mathbf{v}^N}\bigg|_{\hat{\mathbf{p}}} \tag{19c}$$

$$F_{14} = -I_{3\times3} \tag{19d}$$

$$F_{22} = \frac{\partial \dot{\mathbf{p}}}{\partial \mathbf{p}}\bigg|_{\hat{\mathbf{p}},\hat{\mathbf{v}}^N} \tag{19e}$$

$$F_{23} = \frac{\partial \dot{\mathbf{p}}}{\partial \mathbf{v}^N}\bigg|_{\hat{\mathbf{p}}} \tag{19f}$$

$$F_{31} = -A_B^N(\hat{\mathbf{q}})[\hat{\mathbf{a}}^B\times] \tag{19g}$$

$$F_{32} = \frac{\partial \dot{\mathbf{v}}^N}{\partial \mathbf{p}}\bigg|_{\hat{\mathbf{p}},\hat{\mathbf{v}}^N} \tag{19h}$$

$$F_{33} = \frac{\partial \dot{\mathbf{v}}^N}{\partial \mathbf{v}^N}\bigg|_{\hat{\mathbf{p}},\hat{\mathbf{v}}^N} \tag{19i}$$

$$F_{35} = -A_B^N(\hat{\mathbf{q}}) \tag{19j}$$

The following derivatives are shown now to lessen the apparent complexity of the following partials:

$$\frac{\partial R_\Phi}{\partial \lambda} = \frac{ae^2 \sin\lambda \cos\lambda}{(1 - e^2\sin^2\lambda)^{3/2}} \tag{20a}$$

$$\frac{\partial R_\lambda}{\partial \lambda} = \frac{3a(1 - e^2)e^2 \sin\lambda \cos\lambda}{(1 - e^2\sin^2\lambda)^{5/2}} \tag{20b}$$

where the partials are defined as:

$$\frac{\partial \dot{\mathbf{p}}}{\partial \mathbf{p}} = \begin{bmatrix} -\frac{v_N}{(R_\lambda+h)^2}\frac{\partial R_\lambda}{\partial \lambda} & 0 & -\frac{v_N}{(R_\lambda+h)^2} \\ -\frac{v_E\sec\lambda}{(R_\Phi+h)^2}\frac{\partial R_\Phi}{\partial \lambda} + \frac{v_E\sec\lambda\tan\lambda}{R_\Phi+h} & 0 & -\frac{v_E\sec\lambda}{(R_\Phi+h)^2} \\ 0 & 0 & 0 \end{bmatrix} \tag{21}$$

$$\frac{\partial \dot{\mathbf{p}}}{\partial \mathbf{v}^N} = \begin{bmatrix} \frac{1}{R_\lambda+h} & 0 & 0 \\ 0 & \frac{\sec\lambda}{R_\Phi+h} & 0 \\ 0 & 0 & -1 \end{bmatrix} \tag{22}$$

$$\frac{\partial \dot{\mathbf{v}}^N}{\partial \mathbf{p}} = \begin{bmatrix} Y_{11} & 0 & Y_{12} \\ Y_{21} & 0 & Y_{23} \\ Y_{31} & 0 & Y_{33} \end{bmatrix} \tag{23}$$

| NED Gravity Model Coefficients | |
|---|---|
| Coefficient | Value |
| $A$ | $9.780327$ |
| $B$ | $5.3024 \times 10^{-3}$ |
| $C$ | $5.8 \times 10^{-6}$ |
| $D$ | $3.0877 \times 10^{-6}$ |
| $E$ | $4.4 \times 10^{-9}$ |
| $F$ | $7.2 \times 10^{-14}$ |

Table 2: NED Gravity Model Coefficients

which is populated with:

$$Y_{11} = -\frac{v_E^2 \sec^2\lambda}{R_\Phi + h} + \frac{v_E^2 \tan\lambda}{(R_\Phi+h)^2}\frac{\partial R_\Phi}{\partial \lambda}$$
$$-2\omega_e v_E \cos\lambda - \frac{v_N v_D}{(R_\lambda+h)^2}\frac{\partial R_\lambda}{\partial \lambda} \tag{24a}$$

$$Y_{13} = \frac{v_E^2 \tan\lambda}{(R_\Phi+h)^2} - \frac{v_N v_D}{(R_\lambda+h)^2} \tag{24b}$$

$$Y_{21} = \frac{v_E v_N \sec^2\lambda}{R_\Phi + h} - \frac{v_E v_N \tan\lambda}{(R_\Phi+h)^2}\frac{\partial R_\Phi}{\partial \lambda}$$
$$+2\omega_e v_N \cos\lambda - \frac{v_E v_D}{(R_\Phi+h)^2}\frac{\partial R_\Phi}{\partial \lambda}$$
$$-2\omega_e v_D \sin\lambda \tag{24c}$$

$$Y_{23} = -v_E\left[\frac{v_N\tan\lambda + v_D}{(R_\Phi+h)^2}\right] \tag{24d}$$

$$Y_{31} = \frac{v_E^2}{(R_\Phi+h)^2}\frac{\partial R_\Phi}{\partial \lambda} + \frac{v_N^2}{(R_\lambda+h)^2}\frac{\partial R_\lambda}{\partial \lambda}$$
$$+2\omega_e v_E \sin\lambda + \frac{\partial g}{\partial \lambda} \tag{24e}$$

$$Y_{33} = \frac{v_E^2}{(R_\Phi+h)^2} + \frac{v_N^2}{(R_\lambda+h)^2} + \frac{\partial g}{\partial h} \tag{24f}$$

This requires the partials of the gravity model given in Eqn. (14) with respect to latitude and height:

$$\frac{\partial g}{\partial \lambda} = A(2B\sin\lambda\cos\lambda - 4C\sin 2\lambda\cos 2\lambda)$$
$$+(2E\sin\lambda\cos\lambda)h \tag{25a}$$

$$\frac{\partial g}{\partial h} = -D + E\sin^2\lambda + 2F \qquad (25b)$$

The final Jacobian is the derivative of the time rate of change of velocity with respect to velocity, which is given by:

$$\frac{\partial \dot{\mathbf{v}}^N}{\partial \mathbf{v}^N} = \begin{bmatrix} Z_{11} & Z_{12} & Z_{13} \\ Z_{21} & Z_{22} & Z_{23} \\ Z_{31} & Z_{32} & 0 \end{bmatrix} \qquad (26)$$

and is populated with:

$$Z_{11} = \frac{v_D}{R_\lambda + h} \qquad (27a)$$

$$Z_{12} = -\frac{2v_E \tan\lambda}{R_\Phi + h} + 2\omega_e \sin\lambda \qquad (27b)$$

$$Z_{13} = \frac{v_N}{R_\lambda + h} \qquad (27c)$$

$$Z_{21} = \frac{v_E \tan\lambda}{R_\Phi + h} + 2\omega_e \sin\lambda \qquad (27d)$$

$$Z_{22} = \frac{v_D + v_N \tan\lambda}{R_\Phi + h} \qquad (27e)$$

$$Z_{23} = \frac{v_E}{R_\Phi + h} + 2\omega_e \cos\lambda \qquad (27f)$$

$$Z_{31} = -\frac{2v_N}{R_\lambda + h} \qquad (27g)$$

$$Z_{32} = -\frac{2v_E}{R_\Phi + h} - 2\omega_e \cos\lambda \qquad (27h)$$

# 5 Results

## 5.1 Filter Error Results

To simulate GPS/INS navigation, one must propagate GPS satellite positions, and the position of the navigating vehicle near a rotating Earth model. From this, position measurements from GPS satellites and rate measurements from an IMU can be simulated.

GPS satellite positions were determined through the propagation of Newton's equation. Initial conditions were computed from ephemeris obtained from the YUMA Almanac provided by the U.S. Coast Guard Navigation Center website: http://www.navcenter.org/gps/almanacs.htm. GPS position measurements were simulated using Eqn. (1)

Nonlinear least squares was used to estimate the initial position and clock bias for the initial condition of the EKF. It typically computes position and clock bias to within 5 m. The true clock bias was set to 100 000 m. Both filters were provided with the same initial position, which is the approximate location of Buffalo, New York:

$$\mathbf{p} = \begin{bmatrix} 42° \\ -78° \\ 10 \text{ m} \end{bmatrix} \qquad (28)$$

where the negative sign for the longitude denotes a position *west* of the Prime Meridian.

The trajectory provided was chosen for a high degree of observability [12]. The attitude rates were simulated as: $\boldsymbol{\omega}_{B/I}^B = \begin{bmatrix} 1200 & 1200 & 1200 \end{bmatrix}^T$, and the acclerations were:

$$\mathbf{a}^N = \begin{bmatrix} 10\cos(0.1t) \\ -20.5\sin(0.05t) \\ 31\sin(0.1t) \end{bmatrix} \qquad (29)$$

The accelerations were generated with respect to time, and the respective rotational accelerations mapped in both the ECEF and NED frames were added to them to generate measurements. For the ECEF frame, this is:

$$\tilde{\mathbf{a}}^B = A_E^B(\mathbf{q})[[\boldsymbol{\omega}_{E/I}^E \times][\boldsymbol{\omega}_{E/I}^E \times]\mathbf{r}^E + 2[\boldsymbol{\omega}_{E/I}^E \times]\dot{\mathbf{r}}^E$$
$$-\mathbf{g}^E + A_N^E \mathbf{a}^N] + \mathbf{b}_a \qquad (30)$$

and for the NED frame it is:

$$\tilde{\mathbf{a}}^B = A_N^B(\mathbf{q})\left[\mathbf{a}^N + \begin{bmatrix} a_N \\ a_E \\ a_D \end{bmatrix}\right] + \mathbf{b}_a \qquad (31)$$

where the noise is incorporated into the bias model $\mathbf{b}_a$ of Eqn. (3), and the NED accelerations due to position and velocity on the Earth ellipsoid. These were integrated with a fourth-order Runge-Kutta algorithm [13]. The initial velocities for both filters were set to $\dot{\mathbf{r}}^E = \begin{bmatrix} 0 & 0 & 0 \end{bmatrix}^T$ and $\mathbf{v}^N = \begin{bmatrix} 0 & 0 & 0 \end{bmatrix}^T$.

Gyros and accelerometers for both filters were simulated using the same model, with the following truth parameters:

$$\mathbf{b}_g = 5°/\text{hour} \qquad (32a)$$

$$\boldsymbol{\eta}_{gv} = N(0, \sigma_{gv}^2) \qquad (32\text{b})$$

$$\boldsymbol{\eta}_{gu} = N(0, \sigma_{gu}^2) \qquad (32\text{c})$$

$$\mathbf{b}_a = 0.05 \text{ m/s}^2 \qquad (32\text{d})$$

$$\boldsymbol{\eta}_{au} = N(0, \sigma_{au}^2) \qquad (32\text{e})$$

$$\boldsymbol{\eta}_{av} = N(0, \sigma_{av}^2) \qquad (32\text{f})$$

here, the spectral densities of the zero-mean Gaussian processes are given as:

$$\sigma_{gv} = 1 \times 10^{-7} \text{rad/sec}^{3/2} \qquad (33\text{a})$$

$$\sigma_{gu} = 1 \times 10^{-7} \text{rad/sec}^{1/2} \qquad (33\text{b})$$

$$\sigma_{av} = 1 \times 10^{-5} \text{m/sec}^{5/2} \qquad (33\text{c})$$

$$\sigma_{au} = 1 \times 10^{-5} \text{m/sec}^{3/2} \qquad (33\text{d})$$

The values of Eqn. (33) are used to populate the process noise covariance matrix $Q$ given in Eqn. (7). The process noise of the clock bias, $b_c$, is zero. This is because $b_c$ has been observed to change very slowly [1]. The non-zero elements represent the dynamics of the biases in the instruments they model. Initial values for gyro and accelerometer biases were set to $\mathbf{b}_g = [\ 0 \quad 0 \quad 0\ ]^T$ and $\mathbf{b}_a = [\ 0 \quad 0 \quad 0\ ]^T$, respectively.

<mark>Realistic simulations of GPS/INS data fusion would simulate GPS data sampled at 1 to 4 Hz and INS data sampled at 25 to 100 Hz. Doing so results only in adding realism to the simulation, and does not allow the investigator more insight into the performance of estimation routines in this study. Since this is true, both GPS and INS data were sampled at 10 Hz for computational efficiency. The language used to program this work is MATLAB.</mark>

Values for the initial covariance were chosen based upon realistic accuracy of initial measurements. The initial attitude covariance was chosen to be 50°. The initial position covariance was set to 25 meters. The velocity elements of the initial covariance were chosen to be 100 meters per second. The gyro bias was chosen as 10 degrees per hour. The accelerometer bias initial covariance was chosen to be 1 m/s². Finally, the initial covariance for the clock bias was chosen as 10 meters.

Figures 3 through 13 show the estimation errors and $3\sigma$ bounds for the states of the NED and ECEF filters. When comparing these plots, the reader should observe convergence time and the $3\sigma$ bounds. Data were simulated to 3600 s, but were only plotted to 500 s to enhance detail. Table 5.1 presents a comparison of the mean values of the $3\sigma$ bounds for both filters. For this table, the mean value of the $3\sigma$ bounds were taken for the time span of $t = 250$s until $t = 3600$s.

The magnitudes of the $3\sigma$ outliers indicate the uncertainty in the estimate [2], [14]. At any point in time, the $\pm 3\sigma$ outliers span 6 standard deviations between which the estimate error should be centered. This is because a $3\sigma$ span encompasses 99.97% of a population centered on the mean. These are computed from the error covariance matrix $P$:

$$P = \begin{bmatrix} \sigma_1^2 & 0 & \cdots & 0 \\ 0 & \sigma_2^2 & \cdots & 0 \\ \vdots & \vdots & \ddots & \vdots \\ 0 & 0 & \cdots & \sigma_n^2 \end{bmatrix} = \begin{bmatrix} \tilde{\mathbf{x}}\tilde{\mathbf{x}}^T \end{bmatrix} \qquad (34)$$

Here, the error covariance is represented as a diagonal matrix, which is indicative of the absence of cross-correlation of errors between states. The value of the $i^{\text{th}}$ state's $3\sigma$ outlier is given by $3\sigma_{k,i} = 3(\tilde{x}_{k,i}\tilde{x}_{k,i})^{1/2}$. Errors and covariance are presented in the same reference frame using the transformations detailed in [3]. This was done to equate the reference in which the comparison is taken. Initial values for $P$ were chosen based on accuracy of initial measurements.

## 5.2 Nonlinearity Test Results

The following section presents the results of a Kolmogorov-Smirnov (KS) test performed on the estimation errors. This test, through analysis of the probability-density function (PDF) of the error signal, describes how Gaussian an error signal [15] is, and is used in many estimation applicaitons [16]. In the case of this work, the KS test is useful for gauging how well the linearization of the kinematics preserves the true motion. For the case of this study, the KS test should provide insight into which of the ECEF or NED parameterizations of the navigation model best preserve Gaussian error signals through linear approximations of the dynamics.

The KS test is a comparison of the distribution of a data set to that of a Gaussian Probability Density Function (PDF), which is described by the

| Mean $3\sigma$ Bound Values | | | |
|---|---|---|---|
| State Error | ECEF | NED | More Accurate |
| Attitude (deg) | $3.7053 \times 10^{-2}$ | $6.3876\times10^{-2}$ | ECEF |
| | $3.7398\times10^{-2}$ | $6.4917\times10^{-2}$ | ECEF |
| | $3.7292\times10^{-2}$ | $6.4966\times10^{-2}$ | ECEF |
| Position (m) | 1.3807 | 2.4355 | ECEF |
| | 1.3183 | 2.5380 | ECEF |
| | 1.6664 | 2.6705 | ECEF |
| Velocity (m/s) | $1.4499\times10^{-1}$ | $2.6025\times10^{-1}$ | ECEF |
| | $1.6408\times10^{-1}$ | $2.9702\times10^{-1}$ | ECEF |
| | $1.8691\times10^{-1}$ | $3.1711\times10^{-1}$ | ECEF |
| Gyro Bias (deg/hr) | 4.3341 | 4.3364 | ECEF |
| | 4.3480 | 4.3250 | NED |
| | 4.3467 | 4.3193 | NED |
| Accelerometer Bias (m/s$^2$) | $2.8187\times10^{-3}$ | $2.7831\times10^{-3}$ | NED |
| | $2.7908\times10^{-3}$ | $2.8045\times10^{-3}$ | ECEF |
| | $2.7842\times10^{-3}$ | $2.8074\times10^{-3}$ | ECEF |
| Clock Bias (m) | $1.9988\times10^{-1}$ | $1.9874\times10^{-1}$ | NED |

Table 3: Mean $3\sigma$ bound values.

curve [1]:

$$f_g(x) = \frac{1}{\sqrt{2\pi\sigma^2}} \exp \frac{-(x-\mu)^2}{2\sigma^2} \qquad (35)$$

where the mean and standard deviation are represented by $\mu$ and $\sigma$, respectively. The integral of this curve is known as the cumulative distribution function (CDF). Next, the greatest difference between the Gaussian CDF and the CDF of the error signal is defined as:

$$D = \max \|F_{\text{data}}(y) - F_N(y)\| \qquad (36)$$

The greater the value of $D$, the larger the difference between a Gaussian CDF and the one calculated from the signal being analyzed. In other words, the value of $D$ indicates the degree of nonlinearity of a given signal through an extended Filter

The KS-test was performed on filter error signals during the convergence interval from 50s to 250s. The results of this are shown in Table 5.2. The ECEF has a lower KS-test $D$ value in more instances than that of the NED filter, indicating that the ECEF filter might converge faster than the NED filter since it reaches a Gaussian error signal in less time.

The KS test was also run for error data after convergence, but it was found that both filter error signals yielded similar KS values. For this reason, those results are not shown here, but can be found in the author's thesis, [17].

| KS Test $D$ Values During the Convergence Interval | | | |
|---|---|---|---|
| State Error | ECEF | NED | More Gaussian |
| Attitude | 0.0932 | 0.2529 | ECEF |
| | 0.1047 | 0.1638 | ECEF |
| | 0.1260 | 0.1665 | ECEF |
| Position | 0.0828 | 0.0582 | NED |
| | 0.0567 | 0.0538 | NED |
| | 0.0252 | 0.0475 | ECEF |
| Velocity | 0.0518 | 0.1121 | ECEF |
| | 0.1429 | 0.0673 | NED |
| | 0.0762 | 0.0323 | NED |
| Gyro Bias | 0.2218 | 0.3246 | ECEF |
| | 0.0992 | 0.2038 | ECEF |
| | 0.0696 | 0.2406 | ECEF |
| Accelerometer Bias | 0.5749 | 0.5517 | NED |
| | 0.4235 | 0.5780 | ECEF |
| | 0.3045 | 0.4783 | ECEF |
| Clock Bias | 0.1141 | 0.1580 | ECEF |

Table 4: KS Test D Values for the ECEF and NED error signals before the filters converged. The error signals of the ECEF filter are more Gaussian for 11 of 16 error states.
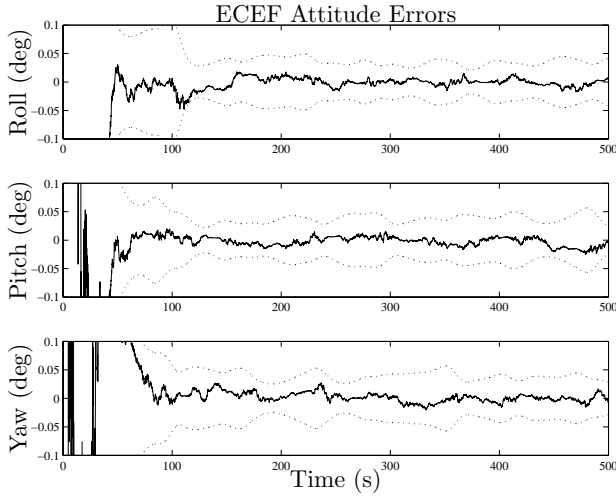


Figure 3: ECEF Attitude Errors and $3\sigma$ outliers with a realistic initial condition.
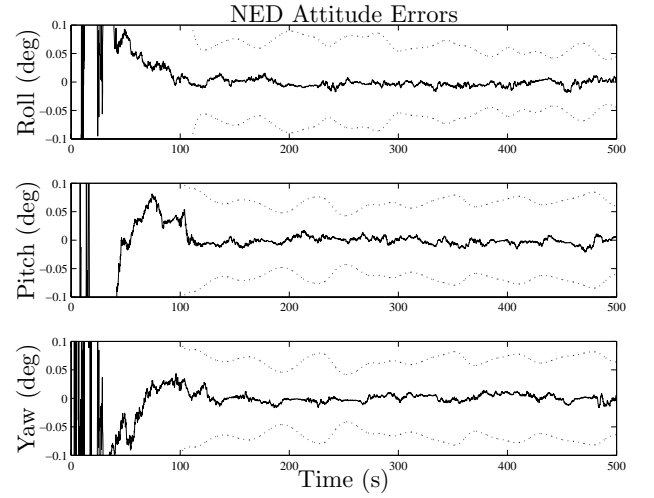


Figure 4: NED Attitude Errors and $3\sigma$ outliers with a realistic initial condition. The NED attitude errors have been represented in ECEF coordinates.

## 6   Discussion

Analysis of the filter errors and covariance presented in the previous section indicate that the ECEF filter performs with higher accuracy. This is supported by the fact that the ECEF converges to smaller $3\sigma$ values for the attitude, position, and velocity states. Both filters, however perform with the same level of accuracy for the bias states.

The ECEF parameterization provided attitude estimates with roughly $4 \times 10^{-2}$ degree $3\sigma$-confidence intervals, while the NED provides the same with $6 \times 10^{-2}$ degree $3\sigma$ confidence intervals.
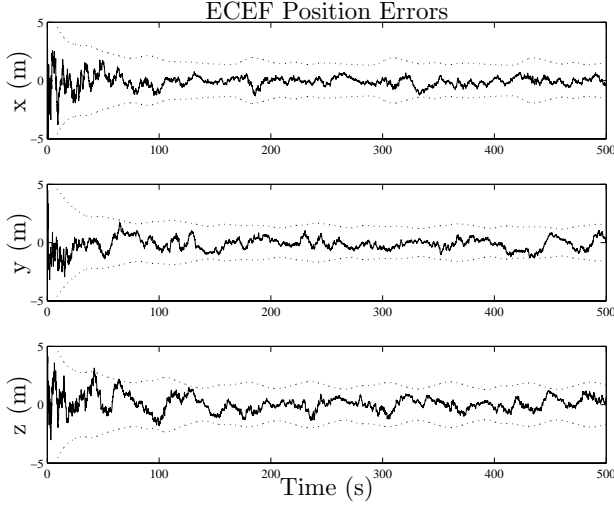
Figure 5: ECEF Position Errors and $3\sigma$ outliers with a realistic initial condition.
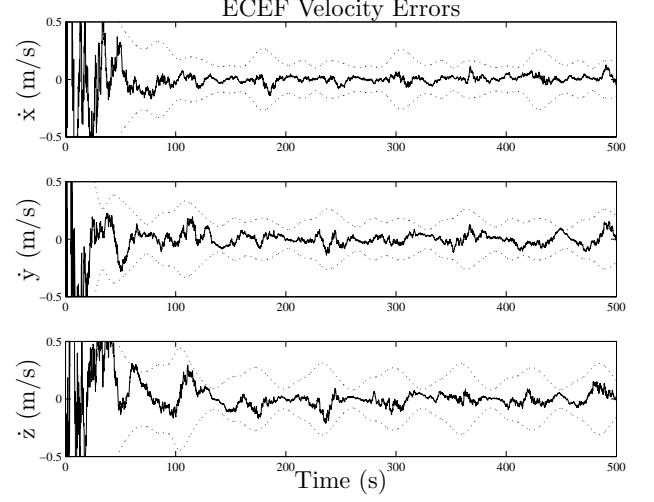


Figure 7: ECEF Velocity Errors and $3\sigma$ outliers with a realistic initial condition.
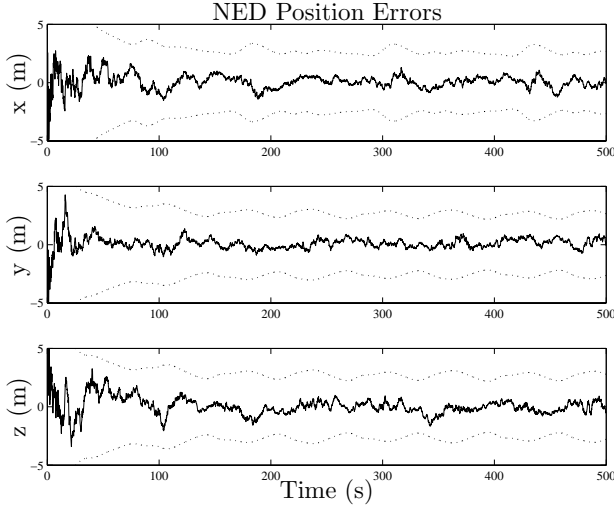


Figure 6: NED position errors and $3\sigma$ outliers with a realistic initial condition. The NED position errors have been represented in ECEF coordinates.
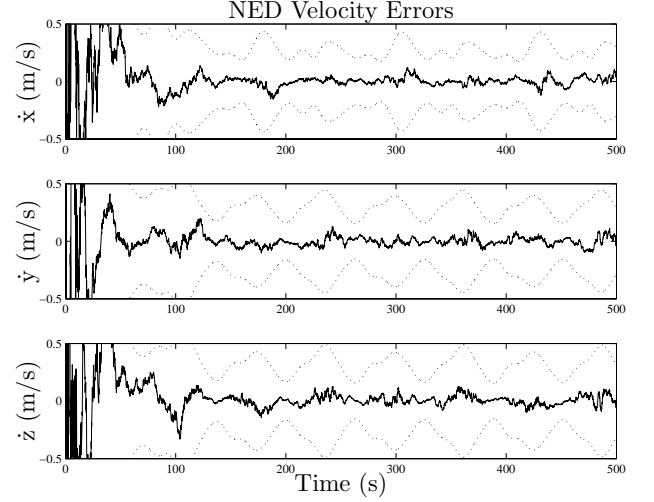


Figure 8: NED velocity errors and $3\sigma$ outliers with a realistic initial condition. The NED velocity errors have been represented in ECEF coordinates.

The ECEF solution produced position estimates with 1.5-meter $3\sigma$ confidence, while the NED parameterization gave the same 2.5-meter accuracy. Finally, the velocities were estimated to 0.15-m/s accuracy by the ECEF filter, and to 0.3-m/s accuracy by the NED filter. Both of these are acceptable for many applications of navigational filtering.

The final three bias states were estimated to the same degree of accuracy by both filters. That is, to 4.3 degrees per hour for the gyro bias, to $2.8 \times 10^{-3}$ m/s$^2$ for the accelerometer bias, and to 0.2 m for the GPS clock bias. In this case, both the NED and ECEF solutions provide the same level of

accuracy, and are equally suited for the task of IMU bias estimation.

An explanation for the higher accuracy of the ECEF filter may lie in Figure 14. Here, the reciprocal of the condition number of the observability matrix is presented for a 10-second time span of the simulation for both filters. The observability matrix for a given system must be full rank if the system is fully observable [18]. The condition number is the ratio of the largest singular value to the smallest singular value of this matrix. The larger the condition number, the more ill-conditioned the observability matrix.
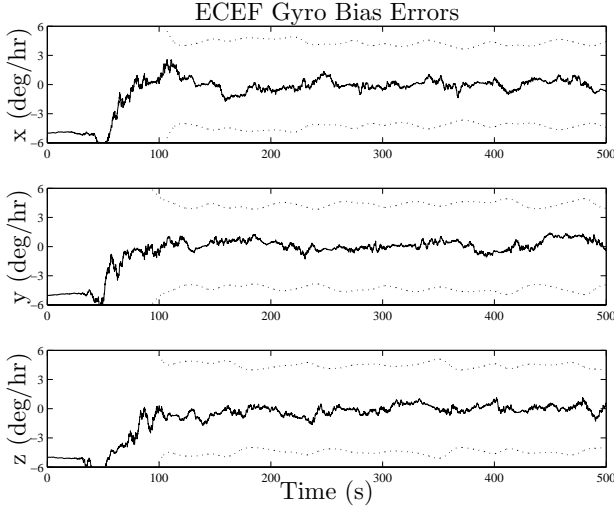
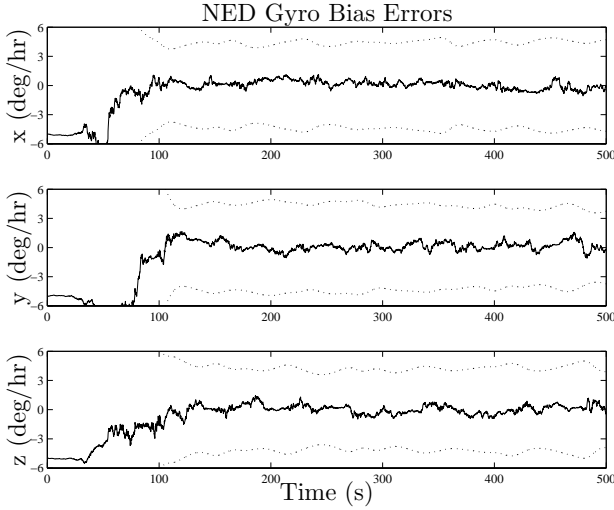Figure 9: ECEF gyro bias errors and $3\sigma$ outliers with a realistic initial condition.



Figure 11: ECEF accelerometer bias errors and $3\sigma$ outliers with a realistic initial condition.



Figure 10: NED gyro bias errors and $3\sigma$ outliers with a realistic initial condition.
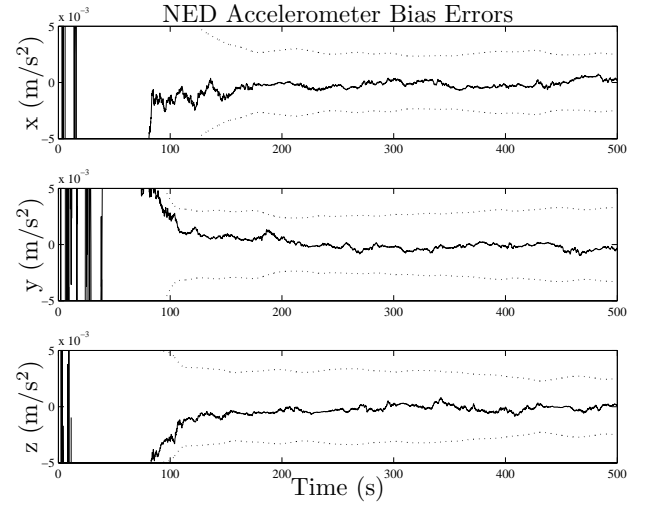


Figure 12: NED accelerometer bias errors and $3\sigma$ outliers with a realistic initial condition.

In Figure 14, the reciprocal of this ratio is presented on a log scale. The small orders of magnitude indicate that the observability matricies of both filters are nearly singular. This means that both systems are nearly unobservable, which illustrates the power of the EKF in estimating otherwise unknown system states.

Also apparent in Figure 14 is that the order of magnitude of the inverse condition number of the ECEF filter is greater than that of the NED filter by several orders of magnitude. This means that the observability matrix for the ECEF filter is conditioned much better than that of the NED filter. Since this test indicates how observable a
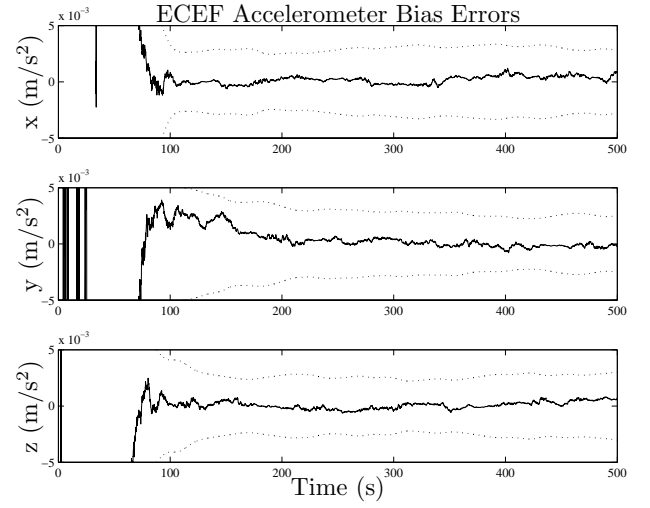
system is, this large difference in condition number may suggest why the ECEF filter yields higher accuracy.

When considering the results of the KS test, one finds that the ECEF filter performed better. Since KS values are an indicator of how Gaussian a given signal is, the KS test results suggest the ECEF filter's linearization better preserves the nonlinear kinematics because it reaches a Gaussian signal faster than the NED filter. After convergence, it was found that both filters yielded similar KS test values which were low enough to suggest that both filters produced nearly Gaussian error signals. This only supports the previous claim that
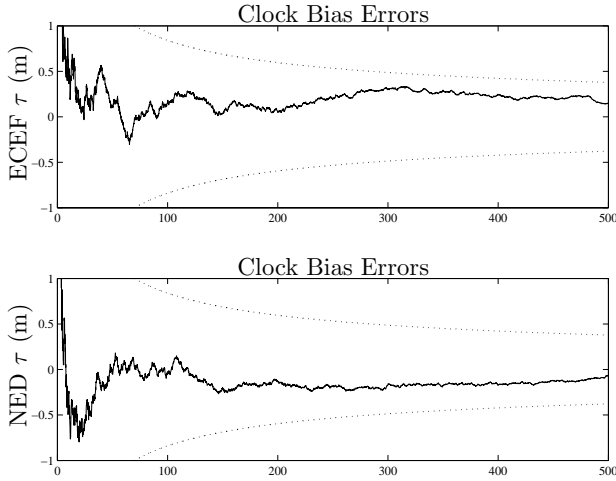
Figure 13: ECEF and NED clock bias errors and $3\sigma$ outliers with a realistic initial condition.
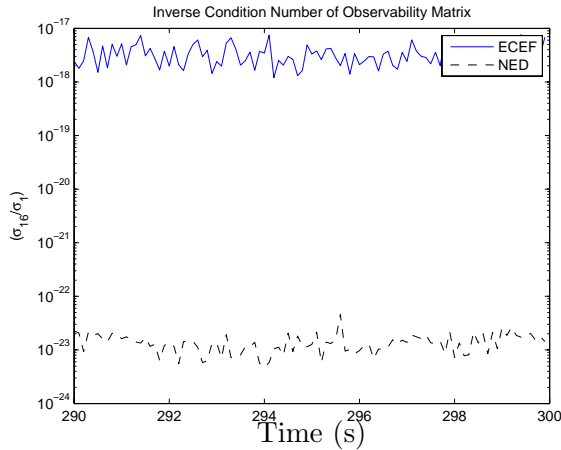


Figure 14: A possible measure of observability.

both versions of the filter are suitable for navigation.

The computational differences of the ECEF and NED routines may provide the programmer with some motivation to choose one over the other. One who wishes to navigate in traditional navigational coordinates might choose the NED parameterization since attitude, position, and velocity will be provided in a local frame. On the other hand, when computational resources are limited, the ECEF filter provides a much simpler parameterization which was found to be 18% faster in this work. The NED dynamics are much more complex than the ECEF equations. This results in a significantly larger computational memory burden. From the perspective of feasibility, therefore, one might be required to use the ECEF parameterization.

# 7   Conclusions

A designer may chose one navigational estimation routine over another for a variety of reasons. In the case of GPS/INS filtering, the EKF was tested in the ECEF and NED frames. Both filters were shown to converge well and yield accurate estimates of INS errors. The NED frame produces data which are readily interpreted in navigation: latitude, longitude, height, and local velocities. The kinematic equations which give this ease of interpretation, however, come with the price of a significantly more complicated computer code and lesser navigational accuracy than the ECEF parameterization. The ECEF frame has been shown to yield higher navigational accuracy, converge faster, and be less computationally burdensome than the NED filter. Even in light of these differences, the decision on whether to use ECEF or NED equations will ultimately depend on the designer and application requirements since both filters are adequately suited for navigation.

# References

[1] Grewal, M., Weill, L., and Andrews, A., *Global Positioning Systems, Inertial Navigation, and Integration*, John Wiley & Sons, Inc., New York, New York, 2001.

[2] Crassidis, J. and Junkins, J., *Optimal Estimation of Dynamic Systems*, Chapman & Hall/CRC, Boca Raton, FL, 2004.

[3] Crassidis, J., "Sigma-Point Kalman Filtering for Integrated GPS and Inertial Navigation," *AIAA Guidance, Navigation and Control Conference and Exhibit, San Francisco, California*, August 2005.

[4] Beyer, J., *Nichtlineare Schätzung inertialer Navigationsgrößen durch die fehlertolerante Verarbeitung zusätzlicher Stützinformationen*, Technische Universität Darmstadt, Darmstädter Dissertation, Darmstadt, Germany, 1993.

[5] Lefferts, E. J., Markley, F. L., and Shuster, M. D., "Kalman filtering for Spacecraft Attitude Estimation," *Journal of Guidance, control, and Dynamics*, Vol. 5.

[6] Hermann, R. and Krener, A. J., "Nonlinear Controllability and Observability," *IEEE Transactions on automatic Control*, Vol. AC-22, No. 6, 1977, pp. 728–740.

[7] Wei, M. and Schwarz, K., "A Strapdown Inertial Algorithm Using an Earth-Fixed Cartesian Frame," *Navigation: Journal of The Institute of Navigation*, Vol. 37, No. 2, Summer 1990, pp. 153–167.

[8] Jekeli, C., *Inertial Navigation Systems with Geodetic applications*, de Gruyter, Berlin, 2001.

[9] Reynolds, R., "Maximum Likelihood Estimation of Stability Parameters for the Standard Gyroscopic Error Model," Tech. Rep. NASA CP-2003-212246, 2003.

[10] Schaub, H. and Junkins, J., *Analytical Mechanics of Space Systems*, American Institute of Aeronautics and Astronautics, Inc., Reston, Virginia, 2003.

[11] Bate, R., Mueller, D., and White, J., editors, *Fundamentals of Astrodynamics*, Dover Publications, New York, NY, 1971.

[12] Goshen-Meshkin, D. and Bar-Itzhack, I., "Observability Analysis of Piece-Wise Constant Systems: Part II: Application and Alignment," *IEEE Transactions on Aerospace and Electronic Systems*, Vol. 28, No. 4, 1992, pp. 1068–1075.

[13] Rao, S., *Applied Numerical Methods for Engineers and Scientists*, Prentice Hall, Upper Saddle River, New Jersey, 2002.

[14] Gelb, A., editor, *Applied Optimal Estimation*, The MIT Press, Cambridge, MA, 1974.

[15] Sinclair, A., Hurtado, J., and Junkins, J., "A Nonlinearity Measure for Estimation Systems," *AAS/AIAA Spaceflight Mechanics Meeting*, January 2006, pp. 22–26.

[16] Najim, K., Ikonen, E., and Daoud, A., editors, *Stochastic Processes: Estimation, Optimisation and Analysis*, Butterworth-Heinemann, New York, NY, July 2004.

[17] Centinello, F., *Analisys of the NED and ECEF Covariance Propagation for the Navigational Extended Kalman Filter*, Master's thesis, University of New York, The State University of New York, Buffalo, New York, 2007.

[18] Chen, C., *Linear System Theory and Design*, Holt, Rinehart and Winston, New York, New York, 1984.